Implications of Mini-EUSO measurements for a space-based observation of UHECRs

Mario Edoardo Bertaina[1,2,*], *Dario* Barghini[1,2,3], *Matteo* Battisti[2], *Alexander* Belov[4,5], *Marta* Bianciotto[1], *Francesca* Bisconti[6], *Carl* Blaksley[8], *Sylvie* Blin[9], *Karl* Bolmgren[10], *Giorgio* Cambiè[6,7], *Francesca* Capel[11], *Marco* Casolino[6,7,8], *Igor* Churilo[12], *Marino* Crisconio[13], *Christophe* De La Taille[14], *Toshikazu* Ebisuzaki[8], *Johannes* Eser[15], *Francesco* Fenu[16], *George* Filippatos[17], *Massimo Alberto* Franceschi[18], *Christer* Fuglesang[10], *Alessio* Golzio[1,2], *Philippe* Gorodetzky[9], *Fumiyoshi* Kajino[19], *Hiroshi* Kasuga[8], *Pavel* Klimov[5], *Viktoria* Kungel[17], *Vladimir* Kuznetsov[12], *Massimiliano* Manfrin[1,2], *Laura* Marcelli[6], *Gabriele* Mascetti[13], *Włodzimierz* Marszał[20], *Marco* Mignone[2], *Hiroko* Miyamoto[2,21], *Alexey* Murashov[5], *Tommaso* Napolitano[18], *Hitoshi* Ohmori[8], *Angela* Olinto[15], *Etienne* Parizot[9], *Piergiorgio* Picozza[6,7], *Lech Wiktor* Piotrowski[22], *Zbigniew* Plebaniak[1,2,20], *Guillaume* Prévôt[9], *Enzo* Reali[6,7], *Marco* Ricci[18], *Giulia* Romoli[6,7], *Naoto* Sakaki[8], *Sergei* Sharakin[5], *Kenji* Shinozaki[20], *Jacek* Szabelski[20], *Yoshiyuki* Takizawa[8], *Giovanni* Valentini[13], *Michal* Vrabel[20], *Lawrence* Wiencke[17], *Mikhail* Zotov[5], and *the* JEM-EUSO Collaboration

[1]Department of Physics, University of Turin, V. P. Giuria 1, 10125 Turin, Italy
[2]INFN Section of Turin, Via P. Giuria 1, 10125 Turin, Italy
[3]INAF Astrophysics Observatory of Turin, Via Osservatorio 20, 10025 Pino Torinese, Italy
[4]Faculty of Physics, M.V. Lomonosov Moscow State University, ul. Kolmogorova 1(2), 119234 Moscow, Russia
[5]Skobeltsyn Institute of Nuclear Physics, Lomonosov Moscow State Univ., ul. Kolmogorova 1(2), 119991 Moscow, Russia
[6]INFN Section of Rome Tor Vergata, Via della Ricerca Scientifica 1, 00133 Rome, Italy
[7]Department of Physics, University of Rome Tor Vergata, Via della Ricerca Scientifica 1, 00133 Rome, Italy
[8]RIKEN, 2-1 Hirosawa Wako, Saitama 351-0198, Japan
[9]Université Paris Cité, CNRS, Astroparticule et Cosmologie, 10 Rue Alice Domon et Léonie Duquet, 75013 Paris, France
[10]KTH Royal Institute of Technology, Brinellvgen 8, 114 28 Stockholm, Sweden
[11]Technical University of Munich, Arcisstraße 21, 80333 Munich, Germany
[12]S.P. Korolev Rocket and Space Corporation Energia, Lenin str., 4a Korolev, 141070 Moscow area, Russia
[13]ASI, Italian Space Agency, Via del Politecnico, 00133 Rome, Italy
[14]Omega, Ecole Polytechnique, CNRS/IN2P3, Rte de Saclay, 91120 Palaiseau, France
[15]Department of Astronomy and Astrophysics, The University of Chicago, 5640 S. Ellis Avenue, Chicago IL 60637, US
[16]Karlsruhe Institute of Technology, Hermann-von-Helmholtz-Platz 1, 76344 Eggenstein-Leopoldshafen, Germany
[17]Department of Physics, Colorado School of Mines, 1523 Illinois St., Golden CO 80401, US
[18]INFN National Laboratories of Frascati, Via Enrico Fermi 54, 00044 Frascati, Italy
[19]Department of Physics, Konan University, 8 Chome-9-1 Okamoto, Higashinada Ward Kobe, Hyogo 658-8501, Japan
[20]National Centre for Nuclear Research, ul. Pasteura 7, 02-093 Warszawa, Poland
[21]Gran Sasso Science Institute, Viale Francesco Crispi 7, 67100 L'Aquila, Italy
[22]Faculty of Physics, University of Warsaw, Ludwika Pasteura 5, 02-093 Warsaw, Poland

Abstract. Mini-EUSO is the first mission of the JEM-EUSO program on board the International Space Station. It was launched in 2019 and it is currently located in the Russian section (Zvezda module) of the station and viewing our planet from a nadir-facing UV-transparent window. The instrument is based on the concept of the original JEM-EUSO mission and consists of an optical system employing two Fresnel lenses and a focal surface composed of 36 Multi-Anode Photomultiplier tubes, 64 channels each, for a total of 2304 channels with single photon counting sensitivity and an overall field of view of $44^\circ \times 44^\circ$. Mini-EUSO can map the night-time Earth in the near UV range (predominantly between 290 nm and 430 nm), with a spatial resolution of about 6.3 km and different temporal resolutions of 2.5 μ, 320 μs and 41 ms. Mini-EUSO observations are extremely important to better assess the potential of a space-based detector in studying Ultra-High Energy Cosmic Rays (UHECRs) such as K-EUSO and POEMMA. In this contribution we focus the attention on UV measurements, the observation of clouds and of certain categories of events that Mini-EUSO triggers with the shortest temporal resolution. We place them in the context of UHECR observations from space, namely the estimation of exposure and sensitivity to Extensive Air Showers.

1 Introduction

The current main goal in the field of UHECR (Ultra-High Energy Cosmic Ray) science is to identify their as-

*e-mail: bertaina@to.infn.it

© The Authors, published by EDP Sciences. This is an open access article distributed under the terms of the Creative Commons Attribution License 4.0 (http://creativecommons.org/licenses/by/4.0/).

trophysical sources and composition [1]. For this, increased statistics is one of the essential requirements. A space-based detector for UHECR research has the advantage of a very large exposure and a uniform coverage of the celestial sphere. The aim of the JEM-EUSO program [2] is to bring the study of UHECRs to space. The principle of observation is based on the detection of UV light emitted by isotropic uorescence of atmospheric nitrogen excited by Extensive Air Showers (EASs) in Earths atmosphere and forward-beamed Cherenkov radiation reected at the Earths surface or at dense cloud tops. The JEM-EUSO program includes missions on ground (EUSO-TA [3]), on stratospheric balloons (EUSO-Balloon [4], EUSO-SPB1 [5], EUSO-SPB2 [6]), and from space (TUS [7], Mini-EUSO [8]) employing fluorescence detectors to demonstrate the feasibility of the UHECR observation from space and prepare for the large size missions K-EUSO [9] and POEMMA [10]. An updated overview of the JEM-EUSO program can be found in [11]. Mini-EUSO is the first detector of the JEM-EUSO program to observe the Earth from the International Space Station (ISS) and to validate from there the observational principle of a space-based detector for UHECR measurements.

2 The Mini-EUSO space telescope

Mini–EUSO (Multiwavelength Imaging New Instrument for the Extreme Universe Space Observatory, known as *UV atmosphere* in the Russian Space Program) [8] is a telescope operating in the near UV range, predominantly between 290 nm and 430 nm, with a square focal surface corresponding to a field of view (FoV) of $\sim 44^\circ \times 44^\circ$. Its spatial resolution at ground level is approximately 6.3×6.3 km^2, slightly varying with the altitude of the ISS and the pointing direction of the pixel. The detector size is $37 \times 37 \times 62$ cm^3, mainly constrained by the size of the nadir-facing UV transparent window in the Russian Zvezda module, where it is attached a couple of times per month during onboard night-time, approximately at 18:30 UTC, with operations lasting about 12 hours. The first observations took place on October 7, 2019. Since then and till October 2022, more than 70 sessions have been performed. Data are stored locally on 512 GB USB pendrives. After each data-taking session samples of data (about 10% of stored data, usually corresponding to the beginning and the end of each session) are copied and transmitted to ground to verify the correct functioning of the instrument and subsequently optimize its working parameters. The pouches containing all stored data are then returned to Earth every ∼12 months by the Soyuz spacecraft.

The optics are based on two 25 cm diameter Fresnel lenses in Polymethyl methacrylate (PMMA). The Mini–EUSO focal surface, or Photo Detector Module (PDM), consists of a grid of 36 Multi-Anode Photomultiplier Tubes (MAPMTs, Hamamatsu Photonics R11265-M64). Each MAPMT consists of 8×8 pixels, resulting in a total of 2304 channels. The MAPMTs are grouped in Elementary Cells (ECs) of 2×2 MAPMTs. MAPMTs are separated by 2 – 3 mm spacing to avoid vibration damage at launch. Consequently, gaps exists between MAPMTs in the collected images. Each EC has an independent high voltage power supply (HVPS) and board connecting the dynodes and anodes of the four photomultipliers. The HVPS system is based on a Cockroft-Walton circuit. The system has an internal safety mechanism which operates either reducing the collection efficiency of the four MAPMTs or reducing the MAPMT gain when particularly bright signals occur (i.e. lightnings or large cities) [8]. The recovery to the nominal mode takes place only few ms after the light level has decreased to a sufficiently low value.

The effective focal length of the system is 300 mm, with a Point Spread Function (PSF) of 1.2 MAPMT pixels. UV bandpass filters (2 mm of BG3 material) with anti-reflective coating are glued in front of the MAPMTs to predominantly select wavelengths between 290 nm and 430 nm.

The system has a single photon-counting capability with a double pulse resolution of ∼6 ns. Photon counts are summed in Gate Time Units (GTUs) of 2.5 μs.

The PDM Data Processor (PDM-DP) stores the 2.5 μs GTU data stream (D1) in a running buffer on which the trigger code is executed. The algorithm searches for a signal integrated over 8 consecutive GTUs above 16 standard deviations from the average in any pixel of the focal surface. Both the average and standard deviation are calculated in real time to take into account varying illumination conditions. In case of a trigger, the 128 frame buffer (64 frames before the trigger and 64 after it) is stored in memory. The choice to operate on 8 GTUs integration and to act on each pixel independently is based on the time needed by a light signal to cross the FoV of a pixel and the fact that 20 μs represent a significant portion of an EAS light-track in atmosphere (see Fig. 1).

Independently from the trigger, sums of 128 frames (320 µs, D2) are continuously calculated and stored in another buffer where a similar trigger algorithm, but at this time scale, is running. Similarly, sums of 128 D2 frames (40.96 ms, D3) are calculated in real time and continuously stored. Every 5.24 s, 128 packets of D3 data, up to 4 D2 packets and up to 4 D1 packets (if triggers were present) are sent to the CPU for storage. In this way various classes of phenomena with different durations can be detected with an appropriate time scale (see sec. 3 for details). A more detailed description of the trigger algorithm is reported in [12], which represents an adaptation of the trigger logic conceived for JEM-EUSO [13], while the onboard performance of the trigger system is summarized in [14].

Prior to the launch, the instrument underwent a series of integration and acceptance tests in Rome, Moscow, and Baikonur cosmodrome, where it was placed in the uncrewed Soyuz capsule. A systematic test of the acquisition logic was performed at the TurLab facility [15] of the University of Turin and at the Astrophysical Observatory of Turin (INAF-OATo) [16].

After launch, an end-to-end in-flight calibration of the Mini-EUSO detector has been performed by assembling different UV-flasher systems on ground in Japan, Italy, and

France and by firing them in various observational campaigns. A detailed description of the methodology and of the observational results is reported in [17].

3 Mini-EUSO design, expected performance and exposure studies

Mini-EUSO has been designed to detect a photon rate per pixel from diffuse sources (nightglow, clouds, cities, etc.) in the range of values expected from a large mission in space such as the original JEM-EUSO mission [18] or the future detectors K-EUSO or POEMMA. The pixel FoV is, therefore, ∼100 times larger in area with respect to the FoV of a JEM-EUSO pixel (∼0.5 × 0.5 km^2), to compensate for the optical system ∼100 times smaller, constrained by the dimension of the UV transparent window (see Fig. 1).

In order to have a precise ratio of the photon rate per pixel from diffuse sources between JEM-EUSO and Mini-EUSO, a full simulation of JEM-EUSO and Mini-EUSO detectors was performed with ESAF simulation software [19]. In case of Mini-EUSO the overall efficiency of the detector was fine-tuned with ESAF, mainly acting at the level of MAPMT response, to match the measured one $\epsilon_{ME} = 0.080 \pm 0.015$ (see the end-to-end in-flight calibration of Mini-EUSO reported in [17]) for a point-like source on ground. A flat diffused UV emission in the range λ = 300 - 400 nm was simulated at the detector's aperture either with a range of zenith directions much larger than the FoV of the instrument (±60° for both detectors) or just within the FoV of the detectors (±30° for JEM-EUSO and ±22° for Mini-EUSO). The estimated background ratio ($R(ME/JE)$) between MiniEUSO and JEMEUSO at FS level is $R(ME/JE) = 0.98 - 1.04$ slightly depending on the range of zenith angles. This result confirms that the expected photon rate from diffuse sources is similar in JEM-EUSO and Mini-EUSO instruments.

The energy threshold of Mini-EUSO for point-like sources like UHECRs is roughly 2 orders of magnitude higher than the original JEM-EUSO one. Fig. 2 shows the trigger efficiency of Mini-EUSO for ESAF simulated proton-generated EASs of different energies. Events have been simulated according to a $\sin(2 \cdot \theta)$ dependence on a larger area than the FoV of the instrument on ground to take into account border effects. The efficiency (ϵ) as a function of the energy (E) has then been calculated as:

$$\epsilon(E) = \frac{N_{trig}}{N_{simu}} \cdot \frac{A_{simu}}{A_{FoV}}, \quad (1)$$

where N_{trig} and N_{simu} represent the number of triggered events over the simulated ones for a specific energy bin, while A_{simu} and A_{FoV} indicate the area on which EAS have been injected and the area on ground in the FoV of Mini-EUSO, respectively. The red and blue points assume a fixed nightglow background of 1 and 2 counts/pix/GTU, respectively. The 50% trigger efficiency is located between 3 - 5 × 10^{21} eV depending on the UV nightglow level.

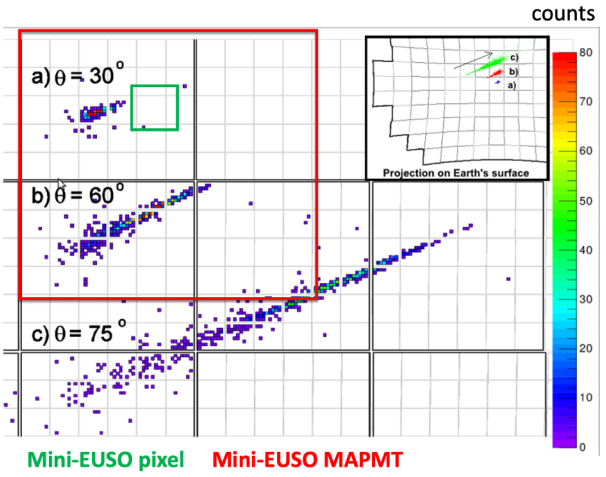

Figure 1. Comparison between JEM-EUSO and Mini-EUSO FoVs. The figure shows the detected light track of three simulated EAS with ESAF [19] of energy 10^{20} eV with different zenith angles (θ = 30°, 60°, and 75°) as imaged by JEM-EUSO detector. Each little colored dot represents the pixel FoV of JEM-EUSO projected on ground, each grey square indicates the MAPMT FoV and the large black squares show the FoV of JEM-EUSO PDMs. The green and red squares represent Mini-EUSO pixel's and MAPMT's FoV, respectively. Mini-EUSO pixel's FoV is larger than the FoV of a JEM-EUSO MAPMT and Mini-EUSO MAPMT's FoV is larger than the FoV of one JEM-EUSO PDM. Image adapted from [18].

Mini-EUSO monitors the atmosphere and studies the nature, extension and duration of the almost steady nightglow emissions and rapid transient lights, to investigate the capability of detecting light signals from EASs and minimize the rate of spurious events. Thanks to its large FoV, Mini-EUSO also acts as an atmospheric monitor detector, observing different natural or anthropogenic phenomena ranging from the UV light reflected or diffused by clouds (D3 data), lightning and thunderstorm activity and study of atmospheric electric phenomena termed Transient Luminous Events (TLEs) [20] with D1 and D2 data, in particular elves, up to much slower events (D3 data) like meteors or, possibly, nuclearites [21], with a sensitivity to fainter events beyond the usual capabilities of atmospheric monitor detectors (see [22] for an updated description of Mini-EUSO results).

Fig. 3 shows a comparison between the cloud fraction (%) due to a cyclone in the Indian ocean as foreseen by a post-processing analysis of the weather forecast obtained with the data collected by the the Global Forecast System of NASA [23], and the Mini-EUSO counts per pixel taken in D3 mode but normalized to the D1 GTU. Where the cloud fraction is expected to be higher, Mini-EUSO registers higher counts level. This is obtained in no-moon condition and shows the capability of the UV camera of Mini-EUSO to detect the presence of clouds. More details can be found in [24]. This is very helpful for the calculation of the exposure and for the determination of the atmospheric conditions in case of the detection of an EAS candidate. A dedicated study to assess the capability of Mini-EUSO

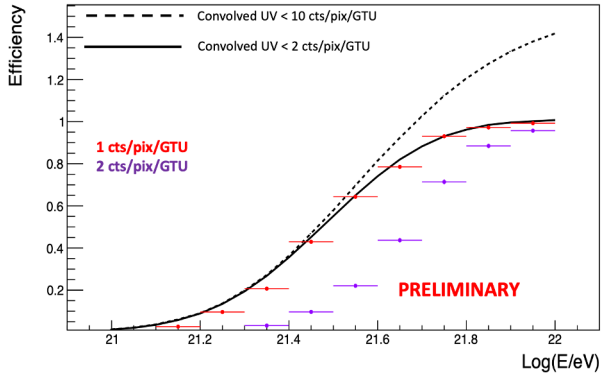

Figure 2. Trigger efficiency curves of Mini-EUSO for ESAF simulated proton-generated EASs of different energies on different background levels. The red and blue points assume a fixed nightglow background of 1 and 2 counts/pix/GTU, respectively. The black line represents the convolved trigger efficiency curve in which each background level below 2 counts/pix/GTU is weighted for the relative fraction of time in which it was measured by Mini-EUSO. The dotted line provides the fractional increase in exposure (relative to the black line) if the accepted nightglow background is increased from 2 counts/pix/GTU to 10 counts/pix/GTU. A significant increase in exposure is obtained only at the highest energies. See text for details.

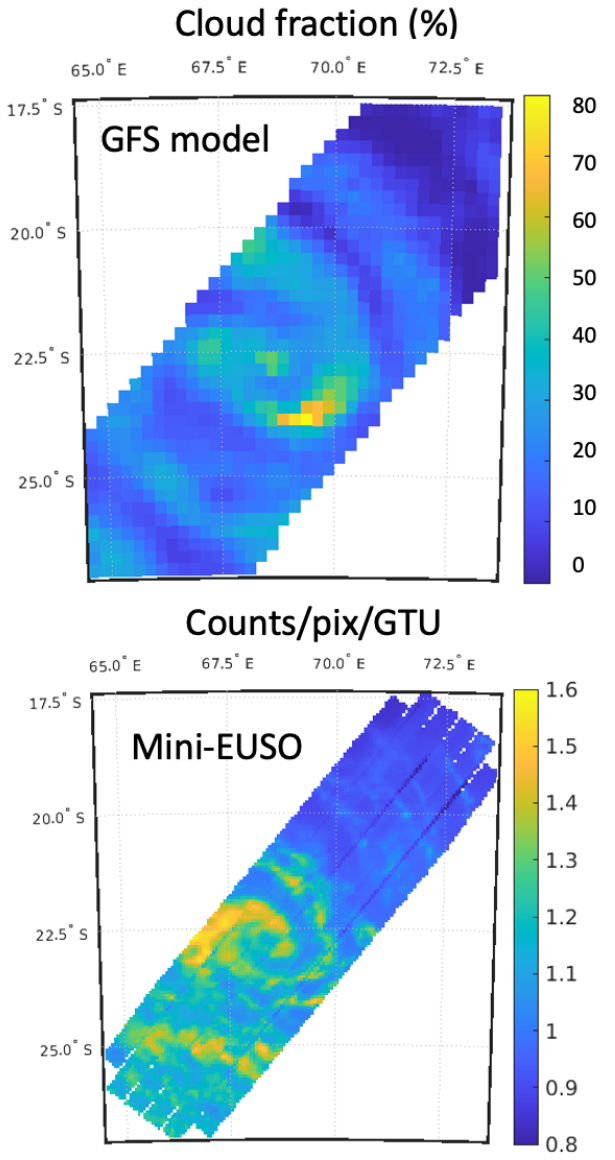

Figure 3. The top panel shows the cloud fraction (%) due to a cyclon in the Indian ocean as foreseen by the GFS atmospheric model [23] and the bottom panel shows the Mini-EUSO counts per pixel and D1 GTU. Where the cloud fraction is expected to be higher, Mini-EUSO registers higher counts level. Figure adapted from [24].

UV camera in recognizing the atmospheric conditions and Mini-EUSO measurements is currently on-going.

The D3 data taken by Mini-EUSO allow a first comparison with the assumed background levels in JEM-EUSO, K-EUSO and POEMMA to verify that the estimated performance is based on justified assumptions. The analysis presented in the following is preliminary as it is based on part of the data collected in 23 sessions between session 05 and 40. A more refined analysis will be performed when all the data collected by Mini-EUSO is available. The weighted moon fraction in those sessions correspond to 0.44 which is well representative of the different moon phases. Fig. 4 shows Mini-EUSO results in terms of UV emission in different conditions: clear and cloudy conditions, sea and land, various lunar phases. A pixel is defined to be in cloudy conditions if the predicted cloud fraction by the GFS model in its FoV is above 1%.

According to Mini-EUSO results in no-moon conditions, in more than 90% of the time of clear sea conditions the count rate belongs to the interval 0.4 - 2.0 counts/pix/GTU, the median being ~0.8 counts/pix/GTU for both clear sea and land conditions. In clear land conditions there is a higher probability of very low counts. These are associated with deserts and forests (see [24] for details). Under the reasonable assumption that conditions above 2 counts/pix/GTU on land are due to the presence of city lights (~20% of the time) and taking into account ~30% land coverage on Earth, this result corresponds to ~6% of the total fraction of time, which is close to the 7% estimation performed for JEM-EUSO in [18]. Moreover, cloudy conditions typically shift curves by a factor 1.5 - 2 towards higher count rates as already measured in JEM-EUSO balloon flights [4]. Taking into account the fact that JEM-EUSO and Mini-EUSO are expected to measure similar count rates from diffuse sources, these results are consistent with the assumption done in [18] for JEM-EUSO where the exposure was calculated under the nominal condition of ~1.1 count/pix/GTU.

Furthermore, when the moon is visible above the horizon, if the moon fraction is less than 0.5, the increase of UV counts is still moderate and it is possible to accumulate exposure at the highest energies.

In order to have a proper estimation of Mini-EUSO exposure at different energies it is necessary to compute an efficiency curve for the various background levels and convolve each efficiency curve with the fraction of time in which such background level is measured. As it is not

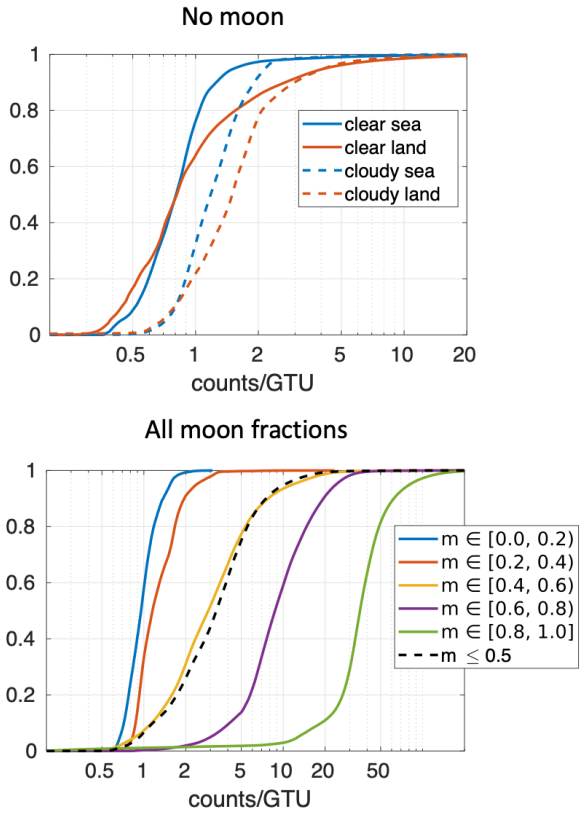

Figure 4. Top: cumulative distributions of Mini-EUSO observations over land and sea regions. Solid lines indicate moonless and cloudless conditions. Dashed lines represent moonless and cloudy conditions, i.e. GFS cloud fraction above 1%. Bottom: cumulative distributions of observations with the Moon visible above the horizon, each curve representing a different moon-phase interval. Figure adapted from [24].

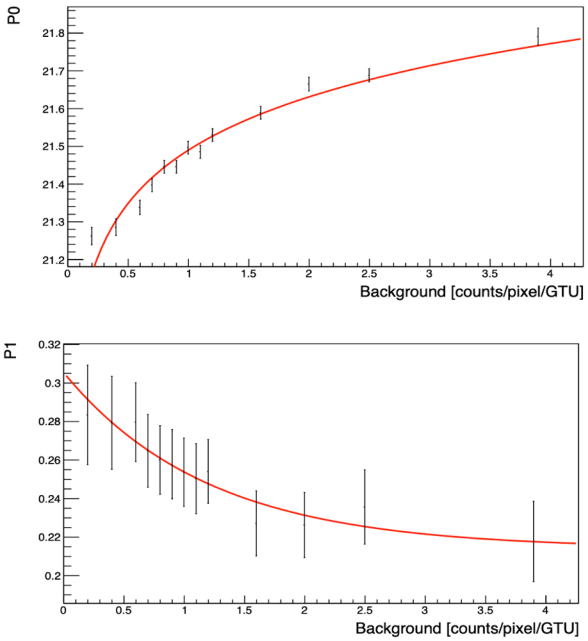

Figure 5. The dependence of the P_0 and P_1 parameters as a function of the background level is displayed. A logarithmic (for P_0) and an exponential function (for P_1) have been used to parametrize their dependence.

possible to simulate the efficiency curves for infinite background levels, as a first step the efficiency curves are estimated by simulated proton-generated EASs of various energies only for a limited set of background levels in the range [0.2;4.0] counts/pix/GTU and the obtained efficiency curves are fitted with a function of the form:

$$\epsilon(E) = 0.5 \cdot [1 + erf(\frac{log_{10}(E/eV) - P_0}{P_1})], \qquad (2)$$

where the parameter P_0 indicates the energy (E) at which the efficiency reaches 50% and P_1 measures the slope of the efficiency curve ($\epsilon(E)$). Subsequently, the obtained parameter values at different background levels have been fitted with appropriate functions as shown in Fig. 5 and the dependencies of P_0 and P_1 as function of the background level have been obtained. Finally, the trigger efficiency curves are modelled at all background levels by equation (2) using as P_0 and P_1 derived by means of the two functions shown in Fig. 5.

Fig. 6 shows the comparison between the efficiency curve obtained by fitting the simulated data points with equation (2) and the efficiency curve, superimposed on the same data points, derived through the parametrization of the P_0 and P_1 dependence for the specific background level of 1 count/pix/GTU. The parameterized curve look very similar to the originally fit.

Finally, the convolved exposure curve ($\mathcal{E}(E)$) has been calculated according to equation:

$$\mathcal{E}(E) = \sum_i (\epsilon_i(E) \cdot t_i \cdot A_i) \cdot \Omega \cdot t_{tot} \cdot \eta, \qquad (3)$$

where i denotes the UV background level, t_i represents the relative fraction of time in which the measured background is in the interval i (each interval having a width of 0.01 counts/pix/GTU), A_i accounts for the cumulative area on ground with background i, Ω measures the UHECR observational solid angle (which assumes the value of π), and t_{tot} = 142.5 hours is the total accumulated time. The parameter η represents the efficiency factor for detecting the EAS maximum in presence of clouds. This value depends on the type of clouds, their optical depth and height. A detailed analysis was performed at the time of JEM-EUSO and adopted in this calculation (η = 60%) and it is applied only to the fraction of time in cloudy conditions. According to Fig. 4 the fraction of time with clear sky and background level below 10 counts/pix/GTU corresponds to ~29% of the total accumulated time, while the fraction in cloudy conditions with similar background conditions corresponds to ~55%. Finally, the exposure curve obtained by integrating all background levels below 2 counts/pix/GTU has been renormalized using the exposure obtained at the plateau level of 10^{22} eV. The result, which represents the convolved trigger efficiency curve, is shown as black line in Fig. 2. The black curve is very close to the efficiency curve obtained at the fixed background level of 1 count/pix/GTU, indicating that such a

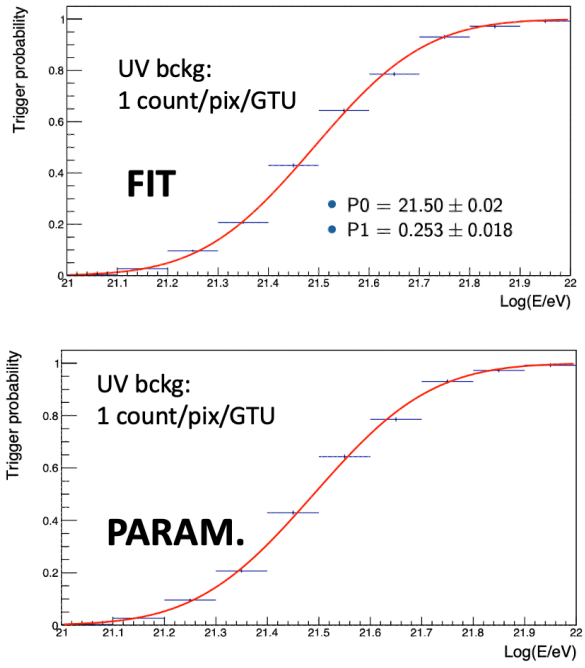

Figure 6. Top: efficiency curve obtained by fitting the simulated data points with equation (2) for the UV background level of 1 count/pix/GTU. Bottom: efficiency curve derived through the parametrization of the P_0 and P_1 dependence as shown in Fig. 5 for the same background level.

curve provides a reasonable approximation of the integrated performance in the various UV background conditions. This result confirms the estimations obtained in the past with JEM-EUSO and the assumptions therein. Similarly, these conclusions can be extended also to the estimation of K-EUSO and POEMMA trigger efficiency curves as they have been derived adopting the very same metodology used for JEM-EUSO.

In addition, if a background level up to 10 counts/pixel/GTU is accepted, at the highest energies the efficiency increases by ~40%. The accumulated exposure of Mini-EUSO in this analysis amounts to 450 Linsley. A very preliminary extrapolation of this result to all good so far recorded data indicates that Mini-EUSO has potentially accumulated till now an exposure equivalent to 2000 Linsley. This value is already about 2% percent of the exposure collected so far by ground-based detectors, roughly 50% in the case of hybrid data [25].

4 Level 1 trigger studies and sensitivity to EAS

A detailed analysis of the events collected by the level 1 trigger logic has been performed on a dataset of 34.7 h containing more than 4.7×10^4 triggered events. The expected functioning of the logic has been confirmed. The trigger rate on spurious events remains within the requirements in nominal background conditions (~1 Hz), while it saturates in the presence of thunderstorm activity. The dead time related to thunderstorm areas corresponds to locations where an UHECR can not be observed due to the presence of high clouds. In that context such dead time issue does not significantly reduce the observation capabilities of a space-based mission. The trigger logic proves effective in avoiding excessive trigger rates in the presence of static anthropogenic lights such as cities confirming the effectiveness of solutions such as the adaptive thresholds, necessary to prevent static light sources from triggering. Several kinds of events are detected such as elves and anthropogenic flashers. All classes of events have characteristics that make them different from an EAS track. However, this trigger capability demonstrates the possibility of a space-based mission to trigger on events with a time duration and light shape similar to, although still different from, what is expected from UHECRs. An example is shown in Fig. 7. The left panel shows a simulated proton-generated EAS of 5×10^{19} eV with a 60° zenith angle as expected to be seen by JEM-EUSO, while the right panel displays a repetitive flasher signal on which Mini-EUSO has triggered near the Missoula city in Michigan, US. The signal intensity at peak level and the integrated number of counts in a limited portion of the events is comparable. This demonstrates the detectability of an EAS light profile in the energy range of interest with a space-based detector.

This kind of anthropogenic signals can be recognized in Mini-EUSO due to the fact that they are repeating several times with a constant time delay (~10 ms for this specific event). Moreover, a careful inspection of the events show a different combination of the shape of the light curve and of the image on the FS when compared to EASs.

One of the most interesting examples of non repetitive flasher-like signals in the Mini-EUSO data sample is shown in Fig. 8. It has been detected off the coast of Sri Lanka. The trigger was issued by the event in the red circle. The lightcurve presents the characteristic bi-gaussian shape of an EAS, with a faster rise and a slower decay time. The event was compared to different simulated EASs with variable energy and zenith angle. No simulated EAS is compatible with both the image size and the time duration of the light profile. In fact, the light spot is compatible with a nearly vertical event, but the duration is much longer than the time needed by a vertical shower to develop in atmosphere and reach the ground. This event has, therefore, a different nature which is currently under investigation. Moreover, the D3 data of Mini-EUSO indicate that the event occurred in a region potentially at the edge between cloudy and clear atmospheric conditions. This observation is supported also by satellite images and GFS analysis and underlines the importance of D3 data to monitor the actual weather conditions when an interesting event occurs.

Finally, we have searched in Mini-EUSO data for EAS-like events such as those detected by TUS and reported in [26]. Fig. 9 shows the comparison between an event produced by a ground flasher detected by Mini-EUSO (red) and the most promising candidate of an UHECR event detected by TUS above Minnesota on October 3rd 2016 (TUS161003 event in blue). The Mini-EUSO event was detected near Traverse City, on the coast of Lake

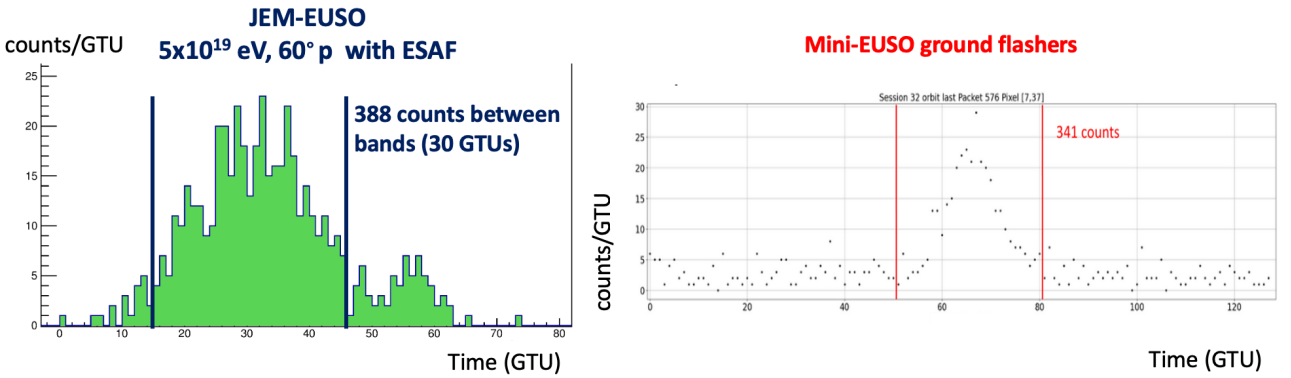

Figure 7. Left panel: a light curve of a simulated proton EAS of 5×10^{19} eV with a 60° zenith angle as expected to be seen by JEM-EUSO (image adapted from [15]). Right side: a light curve of a single flash of a repetitive flasher signal detected by Mini-EUSO near the Missoula city in Michigan, US.

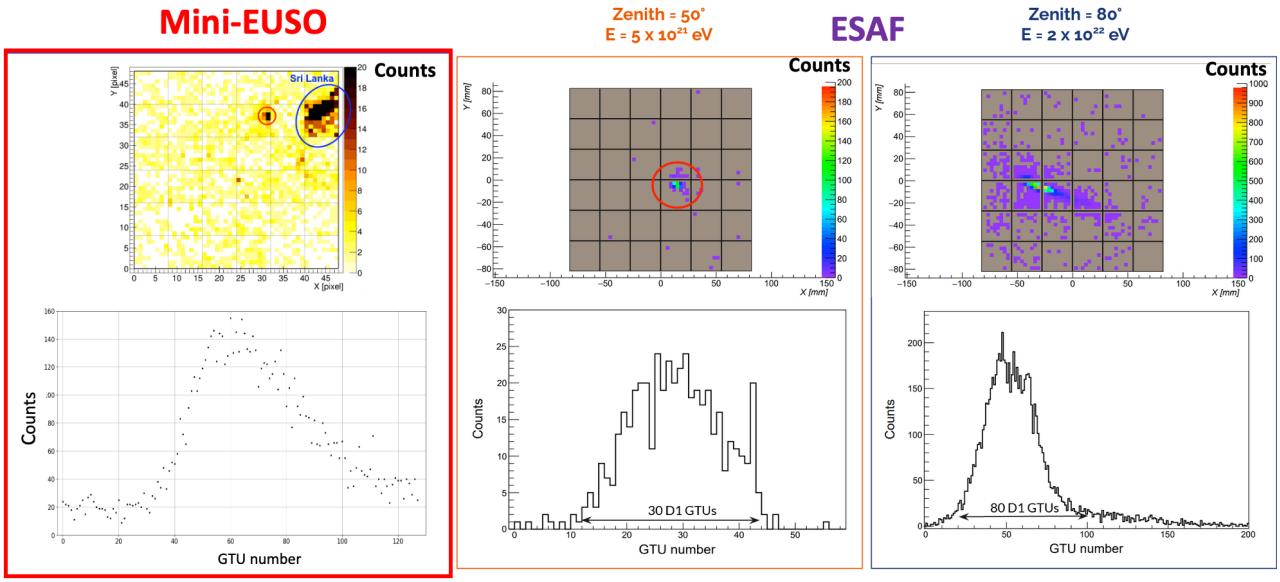

Figure 8. Upper left panel: one frame of an event triggered off the coast of Sri Lanka. The blue circle (upper right) encloses a static, bright light source. The trigger was issued by the event in the red circle. Bottom left panel: the lightcurve of a 3×3 pixel box that contains the event. The lightcurve presents the characteristic bi-gaussian shape, with a faster rise and a slower decay time. Central and right panels: Two proton-generated EAS simulated with ESAF at two different energies and zenith angles (top part presents the image of the events while the bottom part the corresponding lightcurves). The central panel shows a simulation at zenith $\theta = 50°$ and energy $E = 5\times10^{21}$ eV. The signal persists in few pixels for ~30 GTUs, much shorter than the one of measured ground source, the sharp cutoff is given by the shower reaching the ground. The right panel is a simulation with $\theta = 80°$ and primary energy $E = 2\times10^{22}$ eV. The signal is much longer in time but the footprint on the focal plane is much more elongated. Image adapted from [14].

Michigan. The Mini-EUSO event has an anthropogenic nature, because it was triggered four times with a repetition time of ~33 ms, and was found in an area near three small airports. The similar structure of the lightcurve indicated that ground sources can generate light profiles similar to what was detected by TUS, however, we underline that in the TUS161003 event the signal appears to be moving among pixels with a relativistic speed, while in Mini-EUSO data all the signals with a duration compatible with EAS showers appear stationary. More information on the onboard performance of the Mini-EUSO first level trigger and search for EAS-like events can be found in [14].

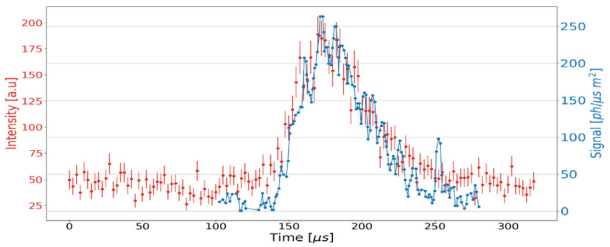

Figure 9. Blue: The lightcurve of the TUS161003 event as seen by TUS [26]. Even though the event has probably an anthropogenic origin, it presents all the features of an EAS signal. Red: An event detected by Mini-EUSO near lake Michigan. It presents the same time profile of the event seen by TUS, even though it is ~10 times brighter. It is produced by a ground source in an area near three small airports. Image adapted from [14].

5 Conclusions

Mini-EUSO is operating on the ISS since more than three years and observes events of different nature demonstrating the multi-disclipinarity of an UHECR detector in space. It shows that it is possible, with larger detectors, to perform UHECR observation from space. Preliminary results indicate that measurements are in agreement with predictions from simulations performed for JEM-EUSO and background issues are under control. These results can be extrapolated directly to K-EUSO and POEMMA and support the outcomes on the instrument performance obtained on those studies.

6 Acknowledgements

This work was supported by the Italian Space Agency through the agreement n. 2020-26-Hh.0, by the French space agency CNES, and by the National Science Centre in Poland grants 2017/27/B/ST9/02162 and 2020/37/B/ST9/01821. This research has been supported by the Interdisciplinary Scientific and Educational School of Moscow University "Fundamental and Applied Space Research" and by Russian State Space Corporation Roscosmos. The article has been prepared based on research materials collected in the space experiment "UV atmosphere". We thank the Altea-Lidal collaboration for providing the orbital data of the ISS.

References

[1] A. Coleman et al., Astrop. Phys. **147** 102794 (2023)
[2] M. Ricci (JEM-EUSO Coll.), J.Phys.Conf.Ser. **718 n.5** 052034 (2016)
[3] G. Abdellaoui *et al* (JEM-EUSO Coll.), Astrop. Phys. **102** 98-111 (2018)
[4] J.H. Adams Jr. *et al* (JEM-EUSO Coll.), Space Sci. Rev. **218** 3 (2022)
[5] L. Wiencke and A. Olinto for the JEM-EUSO Coll., PoS(ICRC2017) **301** 1097 (2017) 1097
[6] J. Eser, A.V. Olinto, L. Wiencke for the JEM-EUSO Coll., PoS(ICRC2021) **395** 404 (2021)
[7] P. Klimov *et al* (TUS Coll.), Space Sci. Rev. **212** 1687-1703 (2017)
[8] S. Bacholle *et al*, ApJS **253** 36 (2021)
[9] P. Klimov *et al* (JEM-EUSO Coll.), Universe **8** 88 (2022)
[10] A. Olinto *et al* (POEMMA Coll.), JCAP **06** 007 (2021)
[11] E. Parizot et al. (JEMEUSO Coll.), This Conference Proceedings (2023)
[12] A. Belov *et al.* (JEM-EUSO Coll.), ASR **62/10** 2966-2976 (2018)
[13] G. Abdellauoi *et al.* (JEM-EUSO Coll.), NIMA **866** 150-163 (2017)
[14] M. Battisti *al.* (JEM-EUSO Coll.), ASR **70/9** 2750-2766 (2022)
[15] P. Barrillon *et al.* (JEM-EUSO Coll.), Exp. Astr. **https://doi.org/10.1007/s10686-022-09871-8** (2022)
[16] F. Bisconti *et al.* (JEM-EUSO Coll.), Exp. Astr. **53/1** 133-158 (2021)
[17] H. Miyamoto et al. (JEMEUSO Coll.), This Conference Proceedings (2023)
[18] J.H. Adams Jr. *et al.* (JEM-EUSO Coll.), Astrop. Phys. **44** 76-90 (2013)
[19] F. Fenu et al. (JEMEUSO Coll.), PoS(ICRC2019) **1472** 252 (2019)
[20] V.P. Pasko et al., Space Sci. Rev. **168** 475-516 (2012)
[21] J.H. Adams *et al.* (JEM-EUSO Coll.) Exp. Astr. **40** 253-279 (2015)
[22] M. Casolino et al. (JEMEUSO Coll.), This Conference Proceedings (2023)
[23] National Centers for Environmental Prediction, National Weather Service, NOAA, U.S. Department of Commerce, 2007, http://dx.doi.org/10.5065/D65Q4TSG.
[24] M. Casolino *et al.* (JEM-EUSO Coll.), Remote Sens. Environ. **284** 113336 (2023)
[25] V. Novotny for the Pierre Auger Coll., PoS(ICRC2021) **395** 324 (2021); H. Shin for the Telescope Array Coll., PoS(ICRC2021) **395** 305 (2021)
[26] B. Khrenov et al. (JEM-EUSO Coll.), JCAP **03** 033 (2020)